Electronic Supplementary Material (ESI) for Materials Chemistry Frontiers.

Supporting Information

Ultrahigh Discharge Efficiency and Energy Density of P(VDF-HFP) via Electrospinning-hot press with St-MMA Copolymer

Jian Wang[a], Yunchuan Xie[a]*, Yifei Zhang[a], Biyun Peng[a], Qizheng Li[a], Denglong Ma[b], Zhicheng Zhang[a]*, Xingyi Huang[c]*

[a] School of Chemistry, Xi'an Key Laboratory of Sustainable Energy Material Chemistry, Xi'an Jiaotong University, Xi'an, Shaanxi 710049, China.

[b] School of Mechanical Engineering, Xi'an Jiaotong University, Xi'an, Shaanxi 710049, China.

[c] Department of Polymer Science & Engineering, Shanghai Key Laboratory of Electrical Insulation & Thermal Ageing, Shanghai Jiaotong University, Shanghai 200240, China.

*Corresponding Authors. E-mails: ycxie@mail.xjtu.edu.cn; (Y.C. Xie)

*Corresponding Authors. E-mails: zhichengzhang@mail.xjtu.edu.cn; (Z.C. Zhang)

*Corresponding Authors. E-mails: xyhuang@sjtu.edu.cn; (X.Y. Huang)

FT-IR analysis

Fig. S1 presents the FT-IR spectra (2400-400 cm^{-1}) of the blend films and pure P(VDF-HFP), where the illustration details the absorption peak of the wave number near 1720 cm^{-1} for comparison with the FT-IR analysis of the composite films in **Fig. 2**.

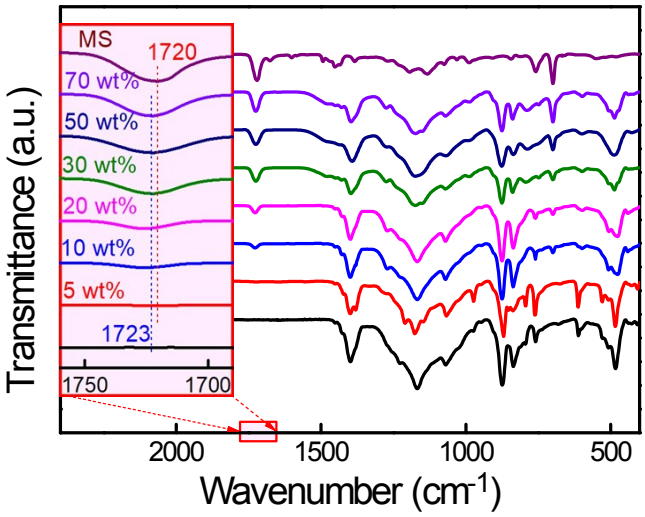

Fig. S1. FT-IR spectra (2400-400 cm^{-1}) of the blend films with different MS contents.

The absorption band at 1720 cm^{-1} is consistent with ester group in MS copolymer, so the peak intensity here in the blend films increases with increasing MS content. The bands of C=O (1720 cm^{-1}) shift to lowered frequency of ~1723 cm^{-1} should be induced by the strong coupling interaction between the P(VDF-HFP) and MS (-C-F····H-C- or -C-H····O-C). However, MS is a homopolymer composed of MMA and St, and due to the action of PS, MS spontaneously agglomerates in PVDF agglomerate to form the island structure in **Fig. 3**, the compatibility of PVDF and MS is poor, thus this deflection is much smaller than that of the composite films, which is attributed to the low number of hydrogen bonds in the blend system. Composite films prepared with the aid of electrospinning-hot press have more hydrogen bonds.

DSC analysis

Fig. S2 presents the DSC heating curves of pristine P(VDF-HFP) and P(VDF-HFP)/MS composite. A double-peak melting process could be observed, which is assigned to melting of α-phase (T_{m1}) and β-phase (T_{m2}) crystal lamellar of P(VDF-HFP), respectively.

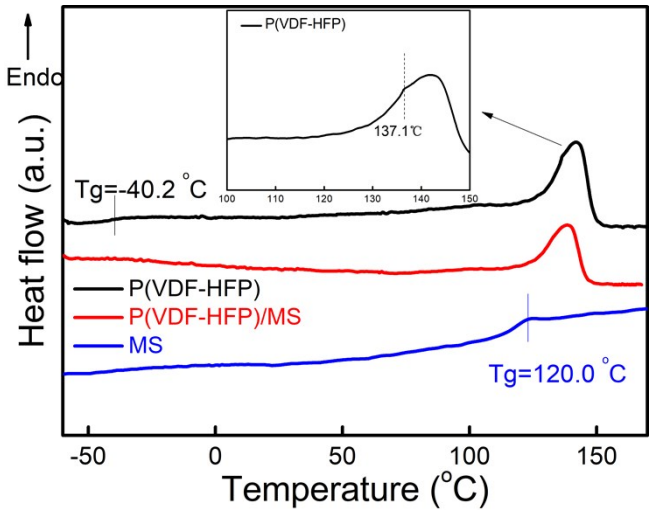

Fig. S2. DSC heating curves of P(VDF-HFP), MS and P(VDF-HFP)/MS (30 wt%) samples.

Table S1. Thermal properties of the composite films derived from the DSC curves in **Fig. 2**d.

Samples	T_{m1} [℃]	T_{m2} [℃]	ΔH_m [J/g]	X_c [%]
P(VDF-HFP)	142.0	137.1	23.2	22.3
5 wt% MS	141.2	137.0	15.9	15.3
10 wt% MS	141.0	136.2	14.1	13.5
20 wt% MS	140.8	134.4	12.8	12.3
30 wt% MS	140.8	134.2	10.0	9.6
50 wt% MS	139.2	/	8.9	8.5
70 wt% MS	135.5	/	4.1	3.9

T_{m1}: melting point of main peak. T_{m2}: melting point of shoulder peak. ΔH_m: melting enthalpy.

X_c: Crystallinity, the melting enthalpy of 100% crystallized P(VDF-HFP) is 104 J/g.

As the MS content increases, the peak temperature of main melting process (T_{m1}) slightly decreases from 142.0 °C to 135.5 °C, and the crystallinity reduces to 3.9% from 22.3% at the same time. This suggests that MS macromolecules could intentively interrupt the chain folding of P(VDF-HFP) segments, which, in turn, reduces the thickness of crystal lamellar and the crystallization degree.

To evaluate the compatibility of P(VDF-HFP) and MS resin, a wide temperature range of DSC analysis was performed and illustrated in **Fig. S2**. It is clear that both P(VDF-HFP) and MS resin present single glass transition temperature (T_g) of around -40 °C and 120 °C, respectively. However, no obvious trace of T_g could be detected during heating process of P(VDF-HFP)/MS (30 wt%) sample, suggesting greatly enhanced compatibility of the two copolymers.

SEM observation

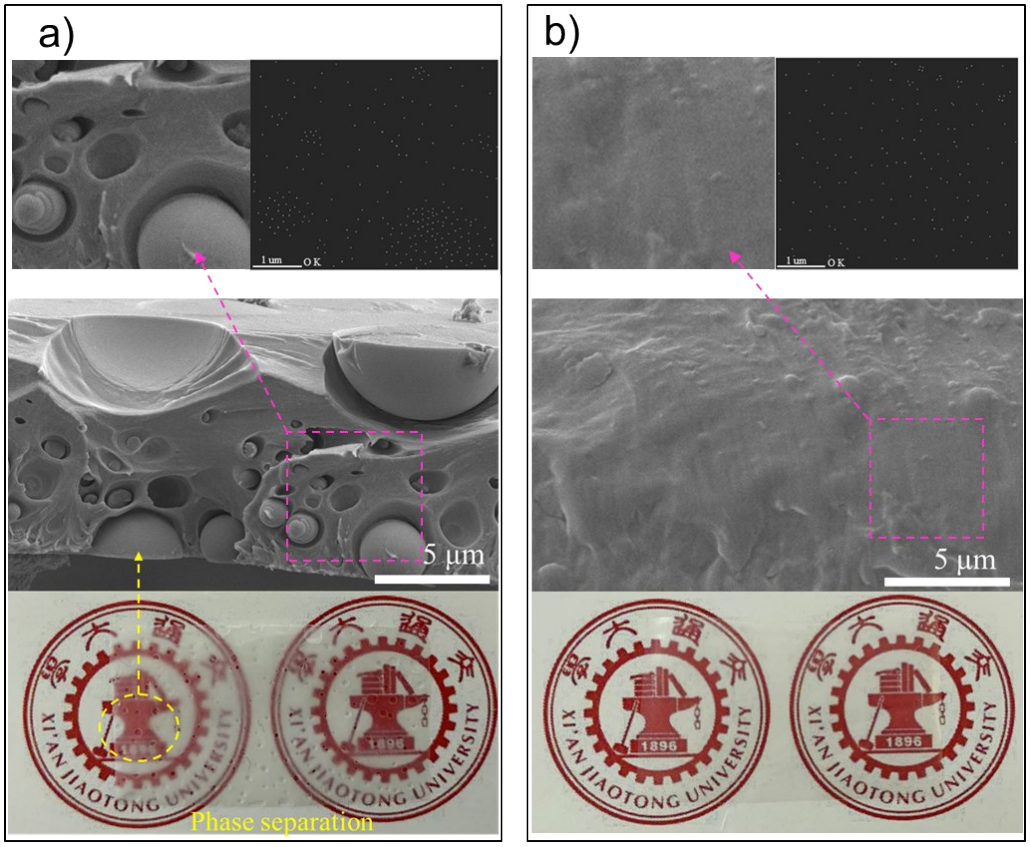

Fig. S3. The EDS elements analysis of oxygen in the cross-sections and optical image of (a) blend films and (b) composite films with 30 wt% MS.

DMA analysis

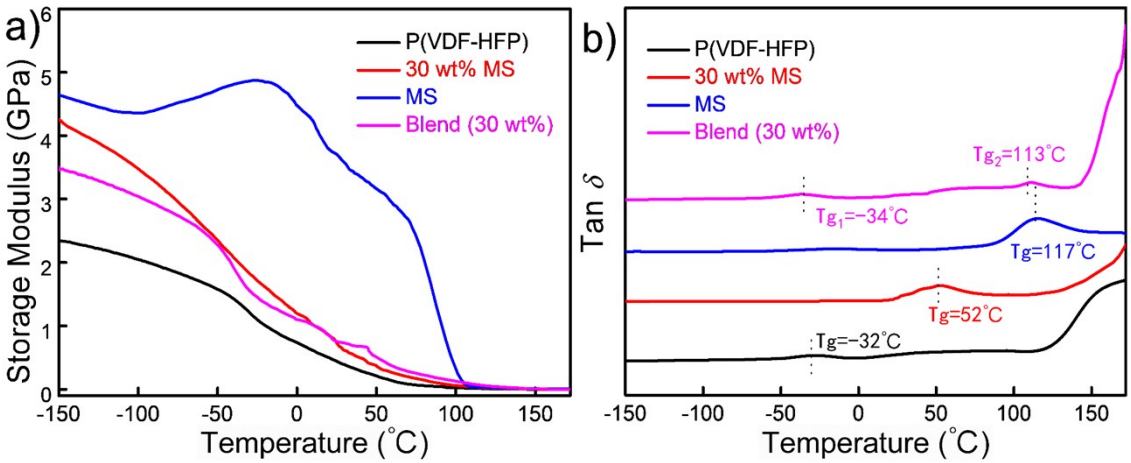

Fig. S4. DMA of P(VDF-HFP), MS and P(VDF-HFP)/MS (30 wt%) samples.

Although no obvious T_g transition could be distinguished in DSC curve of P(VDF-HFP)/MS (30 wt%) composite films [1,2], a single T_g transition is clearly detected in loss tangent of dynamic mechanical analysis (DMA) measurement as shown in **Fig. S4**b. Compared with the two T_g transition in blend films (34 °C, 113 °C), only one T_g transition (52 °C, which is close to calculated value of 66 °C by Fox equation) could be detected in the composite films, which means good compatibility of P(VDF-HFP) and MS copolymer due to strong electrostatic force and confining effect during electrospinning.

Leakage current density

It is noteworthy that, for dielectric materials, the dielectric or electrode interfaces play much more important roles than the dielectrics in determining the leakage current [3,4]. In this work, compared with neat P(VDF-HFP) films, the composite films mitigate the substantially enhanced charge accumulation and exhibit reduced leakage current as presented in **Fig. S5**, this may be attributed to the introduction of high insulating MS resin and strong interactions of the two polymers.

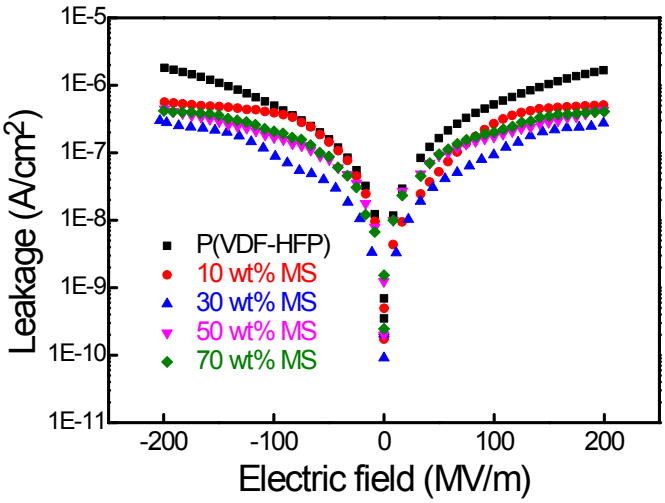

Fig. S5. The leakage current density of different dielectric films at varied electric fields.

Phase field model for dielectric breakdown

A scalar phase field $s(\mathbf{x},t)$ is introduced characterize the damage process in dielectrics [5,6]. Assuming that the ε of dielectrics s η times the original, the ε of solid dielectrics is

$$\varepsilon(s)=\frac{\varepsilon^0}{f(s)+\eta}=\frac{\varepsilon^0}{4s^3-3s^4+\eta} \qquad (1)$$

Define W_{es} is the electrostatic energy stored per unit volume of the dielectrics, $\hat{W}_{es}$ is the complementary electrostatic energy function, $W_i(\nabla s)$ is the gradient energy term to regulate boundaries. The electric trees channel will grow when the electrostatic energy released per unit is greater than the breakdown energy.

$$\Pi[s,\phi]=\int_{\Omega}\left[\hat{W}_{es}(E,s)+W_d(s)+W_i(\nabla s)\right]dV \qquad (2)$$

Assuming the damage rate is proportional to the energy driving force, m is a parameter characterizing the speed of damage propagation in the dielectrics. Substituting in the above energy functions, the evolution equation of the damage variable s is,

$$\frac{1}{m}\frac{\partial s}{\partial t}=\frac{\varepsilon^{'}(s)}{2}\frac{\partial\phi}{\partial x_i}\frac{\partial\phi}{\partial x_i}+W_c f^{'}(s)+\frac{\Gamma}{2}\frac{\partial^2 s}{\partial x_i\partial x_i} \qquad (3)$$

By normalizing all lengths by l, energy densities by W_c, time by $m\Gamma l$, and electric potentials by $\sqrt{\Gamma/\varepsilon^0 l}$, the dimensionless governing equations of s can be written as:

$$\frac{\partial}{\partial\overline{x}_i}\left[\frac{1}{f(s)+\eta}\frac{\partial\overline{\phi}}{\partial\overline{x}_i}\right]=0 \qquad (4)$$

$$\frac{\partial s}{\partial\overline{t}}=-\frac{f^{'}(s)}{2[f(s)+\eta]^2}\frac{\partial\overline{\phi}}{\partial\overline{x}_i}\frac{\partial\overline{\phi}}{\partial\overline{x}_i}+f^{'}(s)+\frac{1}{2}\frac{\partial^2 s}{\partial\overline{x}_i\partial\overline{x}_i} \qquad (5)$$

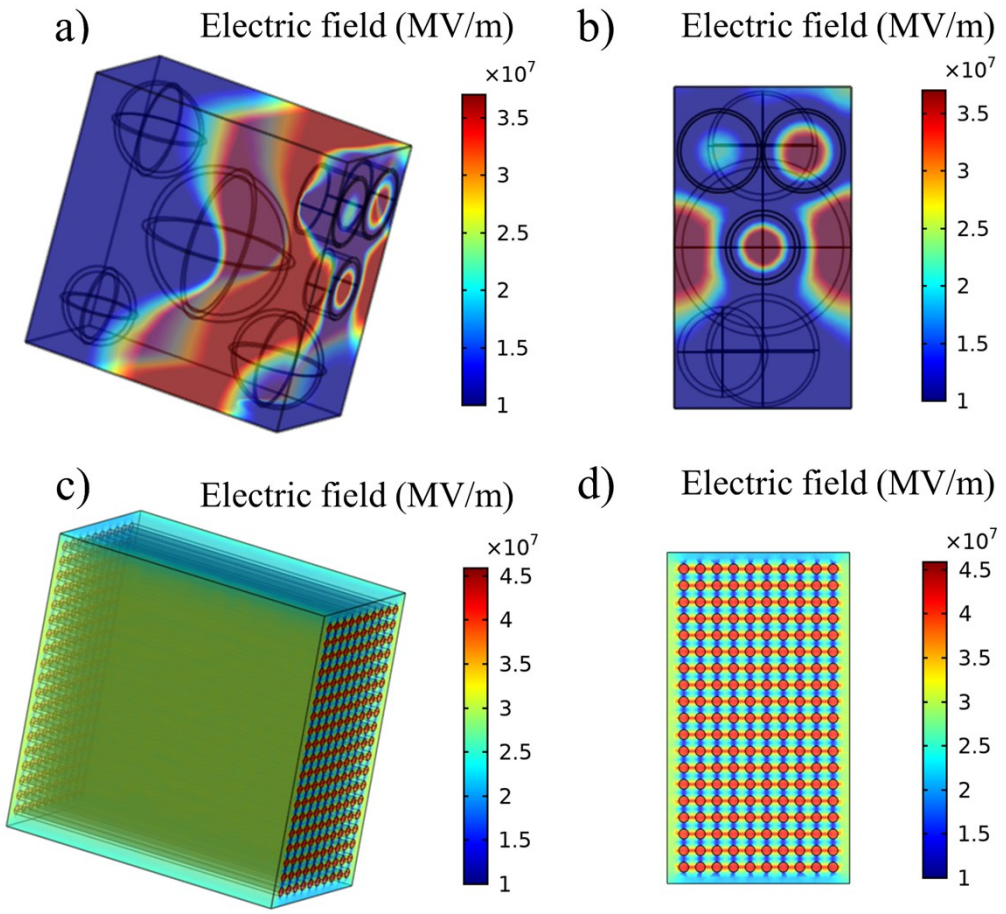

Fig. S6. The corresponding electric field distribution computed by phase-field simulations of (a, b) the blend films and (c, d) the composite films with 30 wt% MS.

D-E loops

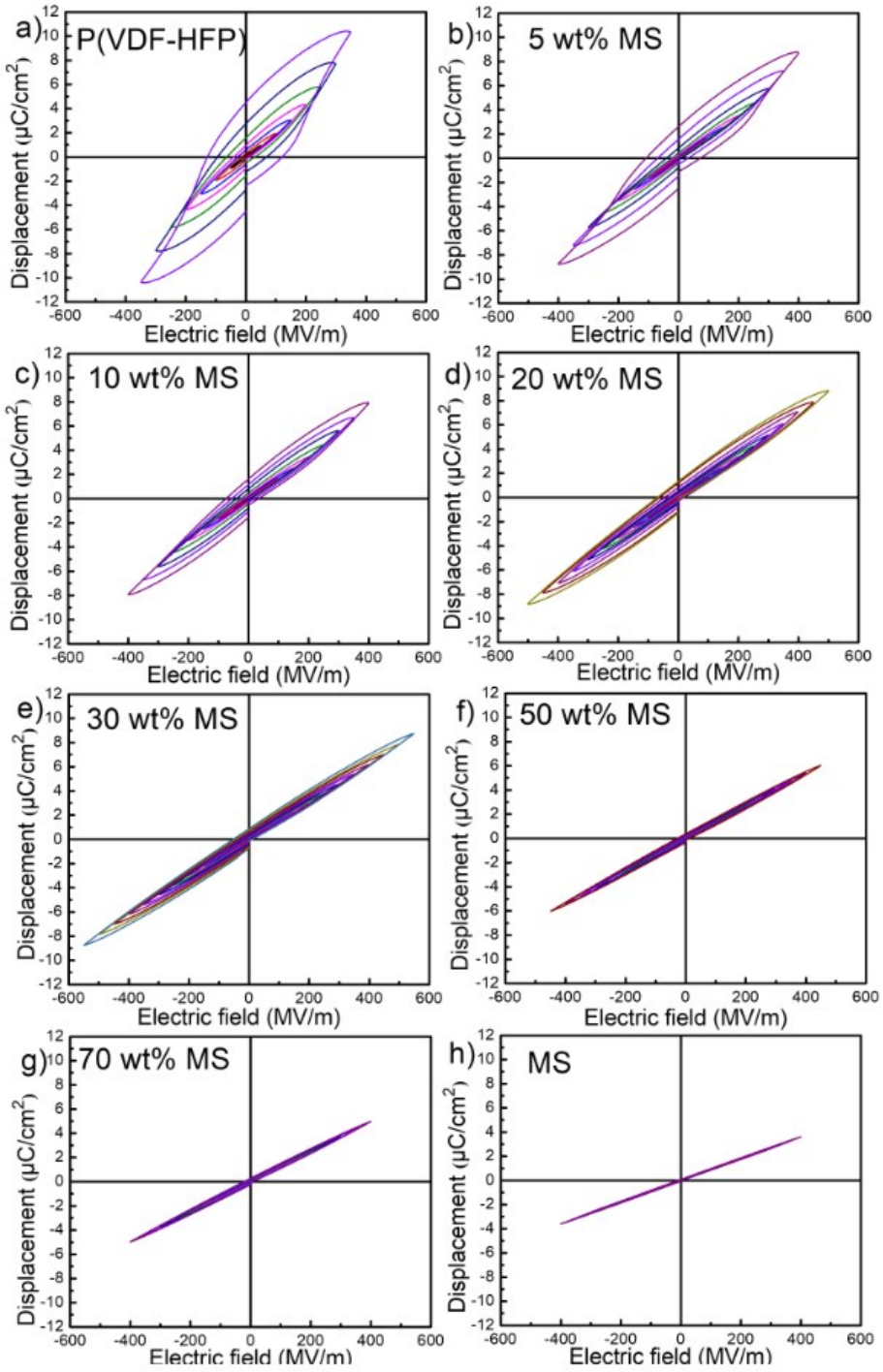

Fig. S7. Bipolar *D-E* loops of (a) pristine P(VDF-HFP), (b-g) composite films with varied MS contents and (h) pristine MS at varied electric fields.

Displacement

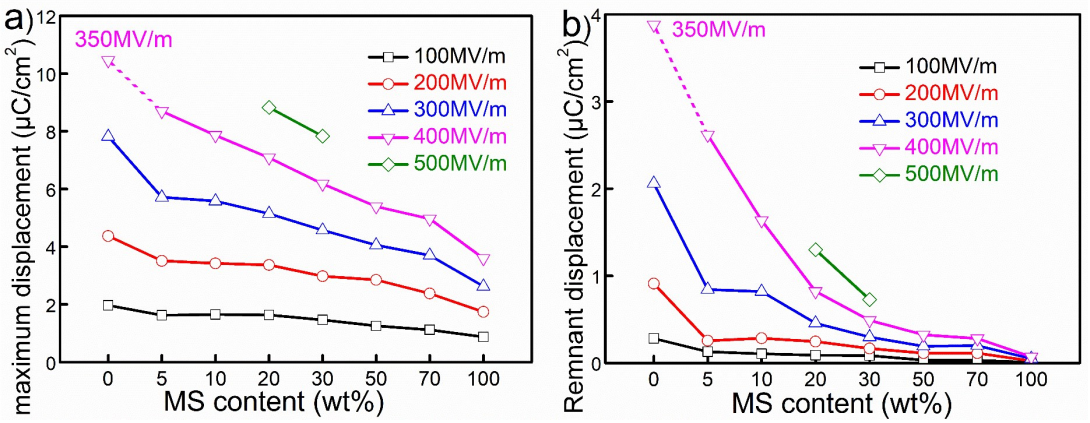

Fig. S8. (a) maximum displacements and (b) remnant displacements of composite films with varied MS fractions.

Significant improvements in capacitive energy storage performance in comparison to neat P(VDF-HFP) could be attributed to the synergetic optimization of decreased maximum displacement and rapidly suppressed remnant displacement. This could be attributed to the synergetic optimization of decreased maximum displacement and rapidly suppressed remnant displacement by tailoring the component ratios, the maximum displacement decreases mildly from ~7.9 μC/cm^2 of P(VDF-HFP) to ~4.8 μC/cm^2 of P(VDF-HFP)/MS (30 wt%) at 300 MV/m, while the remnant displacement substantially decreases from ~2.1 μC/cm^2 to ~0.3 μC/cm^2. Especially, this trend still exists even at an applied electric field, which is beneficial for dielectrics. During the charging process, the maximum displacement offers a high charging energy density under the applied voltages, and the large reduction in remnant displacement confers low loss during discharging, so the introduction of MS gives rise to large enhancements in both U_e and η.

Energy storage density (U_e) and efficiency (η)

The capacitors to store electrical energy is related to its polarization and an externally applied electric field (E). The energy storage density (U_e), energy loss (U_l) and η are expressed as: $U_e = \int_{P_r}^{P_{\max}} EdD$, $U_l = \int_0^{P_r} EdD$ and $\eta = U_e / (U_e + U_l)$, respectively, where P_{max} is the maximum polarization value and is positively correlated with the ε_r of the dielectrics.

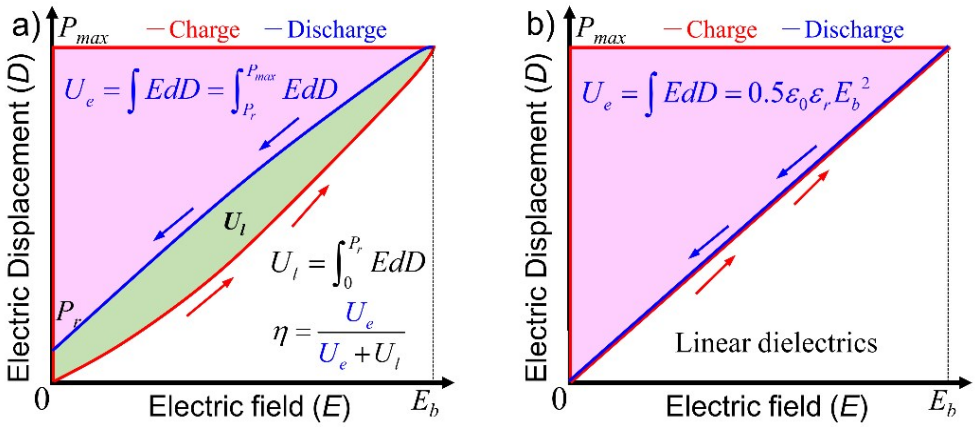

Fig. S9. The schematic diagram of the energy storage performance in *D*-*E* loops.

Dielectric properties of composite films

Table S2. Summary of the electrical and mechanical properties of P(VDF-HFP) and P(VDF-HFP)/MS composite films.

Samples	**Dielectric constant** [a)]	**Young's modulus [Gpa]** [b)]	**Breakdown strength (Experimental/Theoretical)**[c)] **[MV/m]**
P(VDF-HFP)	12.2	0.12	376 / 677
5 wt% MS	8.8	0.25	427 / 804
10 wt% MS	8.1	0.40	448 / 1350
20 wt% MS	7.4	0.60	485 / 1809
30 wt% MS	6.7	0.79	540 / 2189
50 wt% MS	6.4	0.65	480 / 2031
70 wt% MS	4.7	0.42	437 / 1905
MS	3.8	1.00	419 / 3271

a) measured at ambient temperature. b) measured by electromechanical universal testing machine with a 50 N load cell and a stretching rate of 5 mm/min. c) theoretical data was calculated by **Equation S6**.

$$E_b = 0.6 * (Y/\varepsilon_o \varepsilon_r)^{0.5} \qquad \text{(S6)}$$

REFERENCES

1. B. Lu, K. Lamnawar, A. Maazouz and H. G. Zhang, Revealing the dynamic heterogeneity of PMMA/PVDF blends: from microscopic dynamics to macroscopic properties, *Soft Matter.*, 2016, **12**, 3654-3654.
2. B. Hahn, J. Wendorff and D. Y. Yoon, Dielectric-relaxation of the crystal amorphous interphase in poly(vinylidene fluoride) and its blends with poly(methyl methacrylate), *Macromolecules*, 1985, **18**, 718-721.
3. Y. Zhou, Q. Li, B. Dang, Y. Yang, T. Shao, H. Li, J. Hu, R. Zeng, J. L. He and Q. Wang, High-throughput, and environmentally benign approach to polymer dielectrics exhibiting significantly improved capacitive performance at high temperatures, *Adv. Mater.*, 2018, **30**, 1805672.
4. A. Azizi, M. R. Gadinski, Q. Li, M. Abu AlSaud, J. J. Wang, Y. Wang, B. Wang, F. H. Liu, L. Q. Chen, N. Alem and Q. Wang, High-performance polymers sandwiched with chemical vapor deposited hexagonal boron nitrides as scalable high-temperature dielectric materials, *Adv. Mater.*, 2017, **29**, 1701864.
5. H. R. Ye, F. Yang, Z. B. Pan, D. Hu, X. J. Lv, H. X. Chen, F. F. Wang, J. S. Wang, P. Li, J. W. Chen, J. J. Liu and J. W. Zhai, Significantly improvement of comprehensive energy storage performances with lead-free relaxor ferroelectric ceramics for high-temperature capacitors applications, *Acta. Mater.*, 2021, **203**, 116484.
6. W. Hong and K. C. Pitike, Modeling breakdown-resistant composite dielectrics, *Proc. Iutam*, 2015, **12**, 73-82.